VNU Journal of Science: Mathematics - Physics

Journal homepage: https://js.vnu.edu.vn/MaP

Original Article

# Influence of Divalent Electrolytes on the Zeta Potential of Porous Geological Materials

Luong Duy Thanh*, Nguyen Van Nghia, Dang Thi Minh Hue, Tran Thi Chung Thuy

*Thuyloi University, 175 Tay Son, Dong Da, Hanoi, Vietnam*

Received 18th May 2026
Revised 1st July 2026; Accepted 31st July 2026

**Abstract:** Self-potential (SP) signals arising from electrokinetic coupling induced by fluid flow in porous media are widely used in hydrogeophysical and geophysical applications. These signals are fundamentally controlled by the electrical double layer (EDL) at the mineral-fluid interface, in which the zeta potential plays a key role. Accurate determination of zeta potential is therefore essential for quantitative interpretation of SP measurements. In this study, the zeta potential of three porous rock samples (Bentheim sandstone, Berea sandstone, and an artificial ceramic) saturated with divalent electrolytes ($CaCl_2$, $CaSO_4$, and $MgSO_4$) was investigated over a concentration range from $10^{-4}$ to $10^{-2}$ M. The zeta potential was derived by combining measurements of the streaming potential coefficient and electrical conductivity. The results show that the magnitude of the zeta potential systematically decreases with increasing electrolyte concentration for all samples, reflecting compression of the EDL. Significant dependence on both rock type and electrolyte composition is observed: The zeta potential depends strongly on both rock type and electrolyte conditions. In most cases, the natural sandstones exhibit more negative zeta potentials than the artificial ceramic, and $MgSO_4$ generally produces more negative values compared to calcium-based electrolytes, indicating stronger $Mg^{2+}$ surface interactions. In addition, an empirical linear relationship between zeta potential and the logarithm of electrolyte concentration is proposed for divalent electrolytes.

*Keywords:* Streaming potential, zeta potential, porous materials, rocks, divalent electrolytes.

## 1. Introduction

The interaction between fluids and porous media governs a wide range of geophysical and environmental processes, including groundwater flow, hydrocarbon recovery, and contaminant transport. In such systems, electrokinetic phenomena are largely governed by the zeta potential at the

* Corresponding author.
*E-mail address:* thanh_lud@tlu.edu.vn

https//doi.org/10.25073/2588-1124/vnumap.5148

solid-fluid interface, which reflects the properties of the electrical double layer (EDL). Consequently, accurate knowledge of the zeta potential is essential for interpreting streaming potential, electroosmosis, and related geophysical signals.

Self-potential (SP) measurements, arising from electrokinetic coupling, have been widely used to investigate subsurface fluid flow in a variety of geophysical and hydrogeological contexts. Recent studies show that SP data can be effectively applied to delineate flow pathways and to monitor processes such as tracer transport, saline intrusion, hydrothermal circulation, and contaminant migration, thereby providing quantitative insights into the dynamics and spatial distribution of fluid movement [1-4]. Beyond qualitative imaging, SP methods have increasingly been used to estimate key hydrogeological parameters, including hydraulic conductivity and aquifer geometry [5, 6] as well as to monitor emerging applications such as $CO_2$ geological storage, where changes in pore-water chemistry modify electrokinetic coupling [7, 8].

Among the mechanisms contributing to SP signals, the streaming potential is of primary importance in hydrogeological systems due to its direct dependence on fluid flow. Reliable quantitative interpretation of SP data therefore requires accurate estimation of the zeta potential, which governs the electrokinetic coupling at the solid-fluid interface [1].

Most experimental studies of streaming potential and zeta potential in porous media have predominantly focused on systems saturated with monovalent electrolytes, such as NaCl and KCl, for which both experimental datasets and theoretical descriptions are relatively well established [e.g., 9-14]. However, natural groundwater systems typically contain significant concentrations of divalent ions, including $Ca^{2+}$, $Mg^{2+}$, $SO_4^{2-}$, and $CO_3^{2-}$, whose electrochemical behavior differs fundamentally from that of monovalent species. In particular, divalent ions induce stronger electrical double layer (EDL) compression, enhanced surface charge screening, and more pronounced specific adsorption at mineral surfaces, resulting in substantial modifications of zeta potential and electrokinetic coupling.

Recent studies have further shown that ion-specific effects, hydration structure, and surface complexation reactions play a crucial role in controlling electrokinetic responses in multivalent electrolyte systems. As a result, the dependence of zeta potential on electrolyte concentration and composition in divalent systems can deviate significantly from trends established for monovalent electrolytes [15, 16]. Despite these advances, systematic experimental investigations of zeta potential in natural porous rocks saturated with divalent electrolytes remain limited, particularly over a wide range of concentrations and for different mineralogical compositions. This lack of data restricts the development of robust models for interpreting electrokinetic phenomena under realistic groundwater conditions.

This study extends our previous work, in which the streaming potential coefficient (SPC) of consolidated rocks saturated with three divalent electrolytes was measured over a range of concentrations [17]. By combining the measured SPC with electrical conductivity data for each rock sample, the corresponding zeta potentials are derived. In addition, an empirical relationship between zeta potential and electrolyte concentration for divalent electrolytes is proposed, which, to our knowledge, has not yet been reported in the literature. The proposed relationship exhibits a functional form similar to those established for monovalent electrolytes, while variations in zeta potential among the investigated rocks can be qualitatively attributed to differences in mineral composition. By providing zeta potential estimates under realistic groundwater chemistries, this study contributes to a more comprehensive understanding of electrokinetic properties in porous rocks and supports improved interpretation of streaming potential signals in geophysical and hydrogeological applications.

## 2. Theoretical Background of Streaming Potential

In porous geological materials mineral surfaces typically acquire a net negative charge when in contact with an aqueous electrolyte. This surface charge leads to the electrostatic attraction of counter-ions from the pore fluid, resulting in the formation of an EDL at the solid-fluid interface. In its simplest conceptual representation, the EDL consists of two regions: (i) a layer of immobile charges adsorbed onto the mineral surface and (ii) a diffuse layer of mobile ions whose concentration gradually decreases toward the bulk pore fluid. A schematic illustration of this charge distribution is shown in Fig. 1 (see [18] for a detailed description).

The zeta potential ($\zeta$) is defined as the electrical potential at the shear plane that separates the immobile surface charges from the mobile ions in the diffuse layer. As a key electrokinetic parameter, the zeta potential governs the coupling between fluid flow and charge transport in porous media. When a pressure gradient is applied across a water-saturated rock sample, mobile ions in the diffuse layer of the EDL are transported by the flowing fluid, generating a streaming current. The resulting charge separation induces an electric field, which gives rise to a measurable electrical potential known as the streaming potential.

Under steady-state conditions, the SPC is defined as the ratio between the electrical potential difference generated by fluid flow and the applied pressure difference across the porous sample [e.g., 9, 10, 15]:

$$C_S = \frac{\Delta V}{\Delta P}, \tag{1}$$

where $\Delta$V denotes the measured streaming potential and $\Delta$P is the pressure difference imposed across the sample.

The SPC arises from electrokinetic coupling between fluid flow and charge transport and is controlled by both the zeta potential and the physical properties of the pore fluid. Assuming laminar flow and an electrical double layer that is thin relative to the pore size, the SPC can be described by the classical modified Helmholtz–Smoluchowski (HS) equation [e.g., 9, 10, 15, 18]:

$$C_S = \frac{\varepsilon_r \varepsilon_0 \zeta}{\eta \sigma_{\text{eff}}}, \tag{2}$$

where $\varepsilon_r$ (unitless) is the relative permittivity of the fluid, $\varepsilon_0$ (F/m) is the vacuum permittivity, $\eta$ (Pa·s) is the dynamic viscosity, and $\sigma_{\text{eff}}$ (S/m) is the effective electrical conductivity of the saturated porous medium.

The effective electrical conductivity of a saturated porous medium accounts for both the bulk pore fluid conductivity, $\sigma_w$ (S/m), and the additional surface electrical conduction associated with EDL. This effective conductivity can be expressed as [e.g., 18]:

$$\sigma_{\text{eff}} = \sigma_w + \frac{2\Sigma_s}{\Lambda}, \tag{3}$$

where $\Sigma_s$ (S) is the specific surface conductance and $\Lambda$ (m) is a characteristic length scale describing the effective pore size of the porous medium. Physically, $\Lambda$ (m) reflects the influence of pore geometry on surface conduction. Surface electrical conduction occurs primarily within the EDL along mineral surfaces; therefore, its relative contribution depends on the ratio of surface area to pore-fluid volume. In porous media with smaller pores, the surface-area-to-volume ratio is larger, increasing the relative importance of surface conduction compared with bulk-fluid conduction. Conversely, in larger pores, electrical transport is dominated mainly by conduction through the bulk pore fluid. As a result, surface conductivity becomes particularly significant in fine-grained or low-permeability materials.

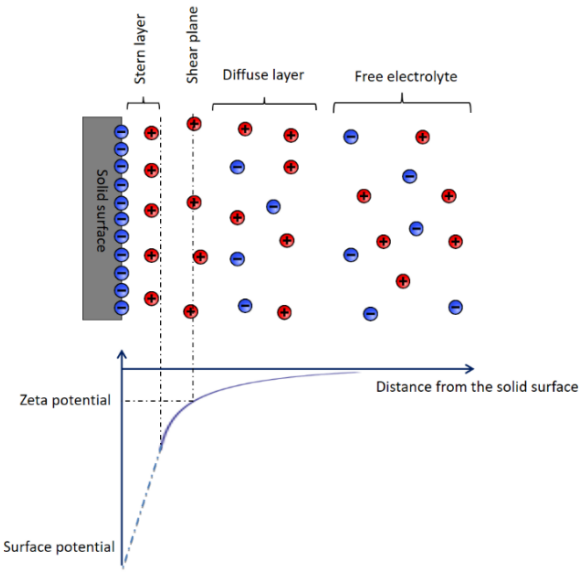


Figure 1. Stern model for the charge and electric potential distribution in the EDL at a solid-liquid interface [e.g., 18].

Alternatively, the SPC may be expressed as [e.g., 15, 18]:

$$C_S = \frac{\varepsilon_r \varepsilon_0 \zeta}{\eta F \sigma_r}, \tag{4}$$

where $\sigma_r$ (S/m) is the electrical conductivity of a sample saturated with a pore fluid of conductivity $\sigma_w$, and $F$ is the formation factor of a porous medium.

As implied by Eq. (4), the zeta potential of a saturated rock sample can be experimentally determined from measured values of $C_S$, $F$, and $\sigma_r$. This relationship provides a practical approach for estimating the electrokinetic properties of porous media, making it particularly useful in laboratory and field-scale applications.

Table 1. Mineral composition, intrinsic permeability $k_0$ (mD) and porosity $\phi$ (%) of the investigated samples

| # | Sample | Mineralogy | $k_0$ | $\phi$ | $F$ |
|---|---|---|---|---|---|
| 1 | S1 | Predominantly silica with feldspar and kaolinite | 1382 | 22.3 | 15.5 |
| 2 | S2 | Fused silica | 430 | 44.1 | 6 |
| 3 | S3 | Silica, Alumina, Ferric Oxide, Ferrous Oxide | 310 | 20.1 | 14,5 |

## 3. Experiment and Results

Based on the theoretical framework of zeta potential and the streaming potential coefficient outlined above, a series of laboratory measurements was conducted on three rock samples - Bentheim sandstone (denoted as S1), Berea sandstone (S2), and an artificial ceramic sample (S3). The samples were saturated with three divalent electrolytes ($CaCl_2$, $CaSO_4$ and $MgSO_4$) at five concentrations: $10^{-4}$ M, $5\times10^{-4}$ M, $10^{-3}$ M, $5\times10^{-3}$ M and $10^{-2}$ M. All measurements were performed at approximately 22°C and pH values ranging from 6.0 to 7.5 under the same experimental conditions as those reported by Thanh and Sprik (2016) [15].

The rock cores were cylindrical, with a diameter $d$ = 2.5 cm and a length $L$ = 5.5 cm. Their mineral composition, as provided by the suppliers, is reported in Table 1. The permeability, porosity, and formation factor of each sample were determined following procedures similar to those reported in [e.g., 15] and are also summarized in Table 1.

The method used to measure the SPC is described in detail in [17]. The SPC values obtained for each sample-electrolyte combination were previously reported in [17] and are reproduced in Table 2 for completeness. As discussed above, determination of the zeta potential additionally requires measurements of the electrical conductivity of the saturated samples ($\sigma_r$). For this purpose, the experimental setup shown in Fig. 2 was employed, following the procedure described below.

The samples were first saturated by continuously circulating the corresponding electrolyte solutions through their pore spaces until full saturation was achieved. The electrical resistance, $R$ (Ω), of each saturated sample was then measured using an impedance analyzer (Hioki IM3570). To ensure reliable electrical contact, two silver mesh electrodes were placed on opposite faces of each sample. The electrical conductivity of the saturated rock sample, $\sigma_r$, was subsequently calculated from the measured resistance together with the sample length, $L$ (m), and diameter, $d$ (m), using the following equation:

$$R = \frac{1}{\sigma_r}\frac{4L}{\pi d^2}. \quad (5)$$

The measured values of $\sigma_r$ for all samples are summarized in Table 3. From the measured values of $C_S$, $F$, and $\sigma_r$, the zeta potential was calculated using Eq. (4). The resulting zeta potential values are presented in Table 4. The average uncertainty associated with the zeta potential measurements was approximately 10%, as reported in [10] for similar experimental measurements.

Table 2. The SPC (mV/bar) measured for the rock samples saturated with different electrolytes at various electrolyte concentrations

| Sample | Electrolyte | Concentration | | | | |
|---|---|---|---|---|---|---|
| | | $10^{-4}$ M | $5\times10^{-4}$ M | $10^{-3}$ M | $5\times10^{-3}$ M | $10^{-2}$ M |
| S1 | $CaCl_2$ | -330 | -102 | -61 | -9.5 | -4.5 |
| | $CaSO_4$ | -363 | -110 | -66 | -22 | -8.7 |
| | $MgSO_4$ | -343 | -160 | -92 | -26 | -13 |
| S2 | $CaCl_2$ | -310 | -95 | -48 | -9.0 | -4.2 |
| | $CaSO_4$ | -297 | -89 | -48 | -10.7 | -5.6 |
| | $MgSO_4$ | -328 | -129 | -67 | -19 | -11 |
| S3 | $CaCl_2$ | -85 | -37 | -23 | -6.7 | -3.1 |
| | $CaSO_4$ | -81 | -35 | -24 | -4.9 | -3.5 |
| | $MgSO_4$ | -83 | -45 | -34 | -12 | -9.0 |

Table 3. Electrical conductivity of samples $\sigma_r$ (mS/m) at different electrolyte concentration

| Sample | Electrolyte | Concentration | | | | |
|---|---|---|---|---|---|---|
| | | $10^{-4}$ M | $5\times10^{-4}$ M | $10^{-3}$ M | $5\times10^{-3}$ M | $10^{-2}$ M |
| S1 | $CaCl_2$ | 0.7 | 1.4 | 2.2 | 10.0 | 18.9 |
| | $CaSO_4$ | 0.9 | 1.3 | 2.1 | 5.2 | 10.2 |
| | $MgSO_4$ | 0.7 | 1.3 | 2.1 | 5.9 | 10.8 |
| S2 | $CaCl_2$ | 1.3 | 2.9 | 4.8 | 21.6 | 37.1 |
| | $CaSO_4$ | 1.2 | 2.9 | 4.8 | 13.5 | 23.2 |
| | $MgSO_4$ | 1.5 | 2.9 | 4.7 | 15.7 | 26.6 |
| S3 | $CaCl_2$ | 1.3 | 2.1 | 3.0 | 10.5 | 18.1 |
| | $CaSO_4$ | 1.2 | 1.9 | 2.8 | 7.5 | 10.9 |
| | $MgSO_4$ | 1.0 | 1.6 | 2.1 | 5.7 | 9.9 |

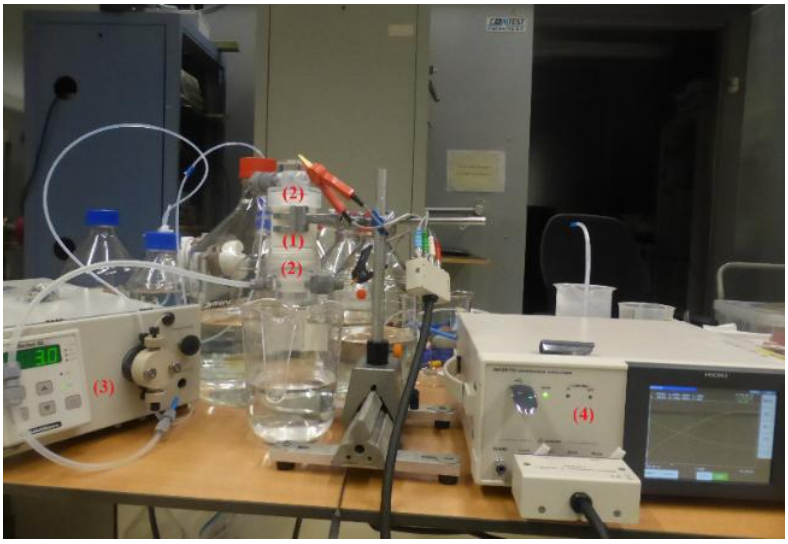


Figure 2. Experimental setup for electrical conductivity measurements: (1) core holder containing the rock sample; (2) positions of the silver mesh electrodes; (3) pump used to saturate the rock samples; and (4) impedance analyzer (Hioki IM3570).

Table 4. Zeta potential ζ (mV) for all samples and electrolytes at different electrolyte concentrations

| Sample | Electrolyte | Concentration | | | | |
|---|---|---|---|---|---|---|
| | | $10^{-4}$ M | $5\times10^{-4}$ M | $10^{-3}$ M | $5\times10^{-3}$ M | $10^{-2}$ M |
| S1 | $CaCl_2$ | -50.5 | -31.2 | -29.3 | -20.8 | -18.6 |
| | $CaSO_4$ | -71.4 | -31.2 | -30.3 | -25 | -19.4 |
| | $MgSO_4$ | -52.5 | -45.5 | -42.2 | -33.5 | -30.7 |
| S2 | $CaCl_2$ | -36.3 | -25 | -24.8 | -17.3 | -14.2 |
| | $CaSO_4$ | -36.8 | -27 | -26.8 | -25.1 | -17.1 |
| | $MgSO_4$ | -43.5 | -39.2 | -36.6 | -34.5 | -29.3 |
| S3 | $CaCl_2$ | -87.7 | -43.8 | -37.4 | -20.4 | -16.7 |
| | $CaSO_4$ | -89.1 | -42.7 | -37.8 | -33.7 | -19.4 |
| | $MgSO_4$ | -70.2 | -52.3 | -39.5 | -30.3 | -23.7 |

The experimental results in Table 4 demonstrate that the zeta potential strongly depends on rock type, electrolyte type, and electrolyte concentration. From the measured $\zeta$ values, the variation in the magnitude of $\zeta$ with rock type and electrolyte concentration is illustrated in Fig. 3: (a) for $CaCl_2$, (b) for $CaSO_4$, and (c) for $MgSO_4$. Figure 3 indicates that increasing the electrolyte concentration leads to a systematic reduction in the magnitude of the zeta potential for all rock types. This trend reflects the progressive compression of the electrical double layer and is in good agreement with previously published results for monovalent electrolytes [9, 10, 15]. Among the investigated samples, Berea sandstone (S2) and Bentheim sandstone (S1) exhibits the more negative surface charge than the artificial ceramic sample (S3). These differences can be attributed to variations in mineral composition and surface chemistry among the samples, which control the density and reactivity of surface charge sites. In particular, the presence of clay minerals and surface heterogeneities in natural sandstones enhances specific interactions with divalent cations, whereas differences in the abundance and nature of reactive surface sites among the investigated materials may lead to different electrokinetic responses.

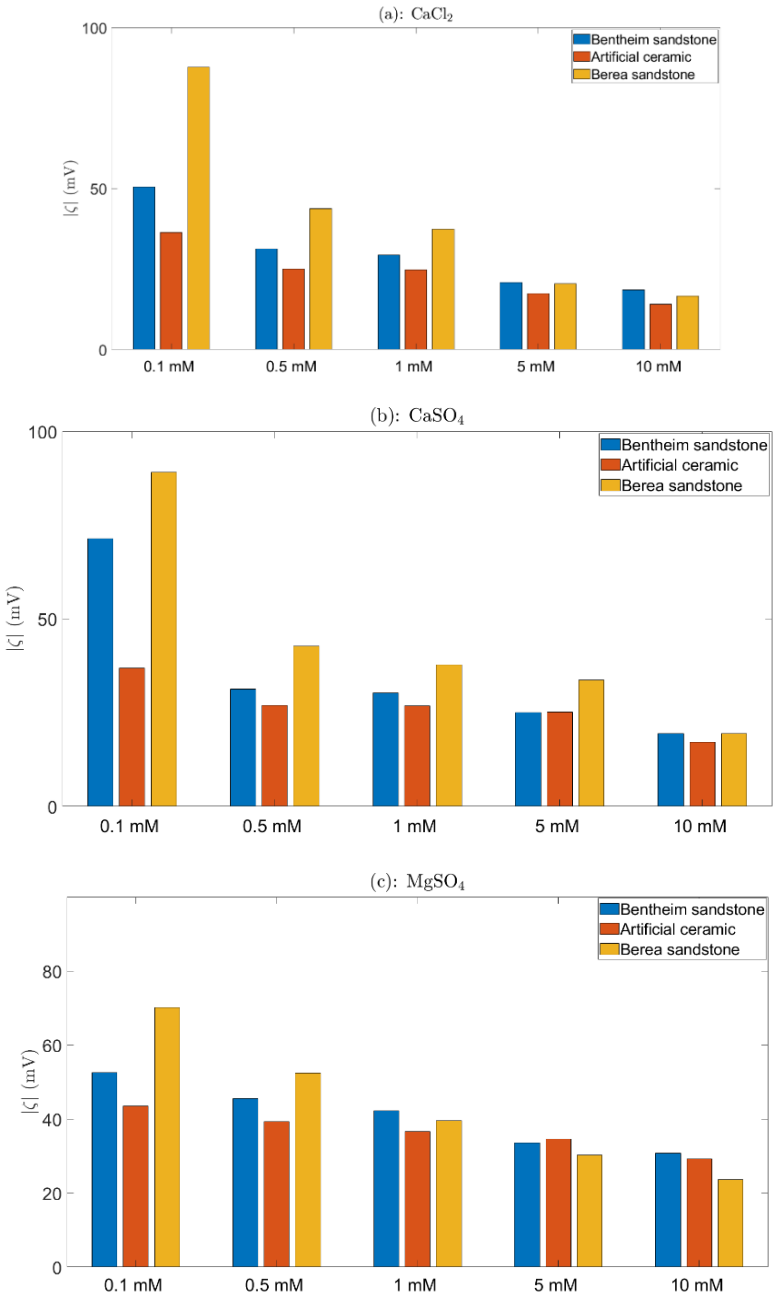


Figure 3. Variation in the magnitude of the zeta potential ($|\zeta|$) with rock type and electrolyte concentration: (a) $CaCl_2$; (b) $CaSO_4$; and (c) $MgSO_4$.

Previous studies have shown that mineral composition, clay content, and surface heterogeneity can significantly influence zeta potential through their effects on surface charge and ion adsorption processes [9, 14, 15, 18]. Therefore, the differences observed among the investigated samples may partly reflect variations in their mineralogical composition. However, because detailed mineralogical characterization

was not performed in this study, this interpretation remains qualitative and is based on the mineralogical information reported in Table 1.

Additionally, $MgSO_4$ mostly produces more negative zeta potentials for the same rock than calcium-based electrolytes except at electrolyte concentration of $10^{-4}$ M, indicating stronger $Mg^{2+}$ adsorption onto mineral surfaces.

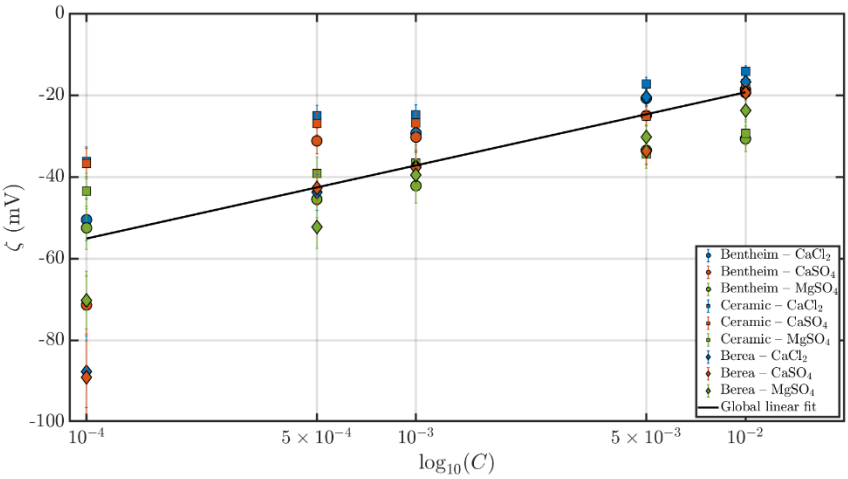


Figure 4. Zeta potential as a function of electrolyte concentration. The solid line represents the best fit of Eq. (6) to the experimental data.

Based on the values reported in Table 4, the zeta potential was plotted as a function of electrolyte concentration for all rock types and electrolytes. Error bars of ± 10% were included to provide an indication of the variability and scatter in the data, as shown in Fig. 4. In electrokinetics and surface chemistry, the zeta potential commonly exhibits a monotonic dependence on the logarithm of electrolyte concentration. Over a limited concentration range, many models predict an approximately linear relationship between the zeta potential and the logarithm of concentration (see, for example, [9] and references therein), which can be expressed as

$$\zeta = a\log_{10}(C) + b, \tag{6}$$

where ζ is expressed in mV and $C$ is the electrolyte concentration in mol/L (M). The coefficients $a$ and $b$ were determined using the ordinary least squares method by minimizing the sum of squared residuals between the measured zeta potentials and the values predicted by Eq. (6). The resulting best-fit parameters are $a$ =17.9, $b$ =16.5, with a coefficient of determination $R^2$ = 0.57.

The zeta potential values obtained in this study are generally consistent with those reported previously for silica-rich sandstones and porous materials saturated with electrolyte solutions. For example, Vinogradov et al., [9] reported zeta potentials ranging approximately from −10 to −40 mV for sandstone samples saturated with NaCl brines over a wide salinity range, while Thanh and Sprik [15] observed zeta potentials between approximately −15 and −60 mV for porous rocks saturated with mono- and divalent electrolytes. More recent studies on quartz-rich materials and sandstone samples have also reported negative zeta potentials whose magnitude decreases with increasing ionic strength due to compression of the electrical double layer [8, 14]. Although direct quantitative comparison is complicated by differences in mineralogy, electrolyte composition, pH, and experimental methodology, the zeta potential values measured in the present study (approximately −14 to −89 mV) fall within the

broader range reported in the literature and exhibit the same overall trend of decreasing magnitude with increasing electrolyte concentration.

It is worth noting that only a limited number of empirical relationships have been proposed in the literature to estimate zeta potential as a function of electrolyte concentration, and these are almost exclusively restricted to monovalent electrolytes. Empirical expressions applicable to divalent electrolytes remain scarce. For example, Vinogradov et al. fitted experimental data for silica-based materials, including sandstones, sand packs, silica nanochannels, Stainton, and Fontainebleau samples, saturated with monovalent NaCl and KCl solutions at pH values between 6 and 8, obtaining fitting parameters $a$ = 19.02, $b$ = −9.67 mV with $R^2$ = 0.71 [9]. In contrast, Eq. (6) and the fitted parameters reported here are directly relevant to systems containing divalent electrolytes, thereby extending existing empirical descriptions to a less explored but practically important regime.

## 5. Conclusions

This study presents an experimental investigation of the zeta potential of consolidated porous rocks saturated with divalent electrolytes, using a combined approach based on streaming potential coefficient and electrical conductivity measurements. Experiments conducted on Bentheim sandstone, Berea sandstone, and an artificial ceramic sample with $CaCl_2$, $CaSO_4$, and $MgSO_4$ solutions over a concentration range of $10^{-4}$ to $10^{-2}$ M demonstrate a systematic decrease in the magnitude of the zeta potential with increasing electrolyte concentration, consistent with progressive compression of the electrical double layer.

The results highlight a strong dependence of zeta potential on both rock type and electrolyte composition. Natural sandstones generally exhibit more negative zeta potentials than the artificial ceramic, which can be attributed to differences in mineralogy and surface charge properties. In addition, $MgSO_4$ tends to produce more negative zeta potentials than calcium-based electrolytes, suggesting stronger specific adsorption of $Mg^{2+}$ ions at mineral surfaces.

An empirical linear relationship between zeta potential and the logarithm of electrolyte concentration is proposed for divalent electrolyte systems. This relationship extends existing empirical models, which are largely limited to monovalent electrolytes, and provides a useful framework for predicting electrokinetic behavior under more realistic groundwater conditions. Overall, these findings contribute to improving the quantitative interpretation of streaming potential signals in porous media and offer valuable constraints for hydrogeophysical applications.

## Acknowledgments

This research is funded by Vietnam National Foundation for Science and Technology Development (NAFOSTED) under grant number 103.99-2023.04. The authors gratefully acknowledge Prof. Rudolf Sprik (Van der Waals-Zeeman Institute/Institute of Physics, University of Amsterdam, The Netherlands) for his support in carrying out part of this work.

## References

[1] A. Revil, A. Finizola, M. Gresse, Self-Potential as a Tool to Assess Groundwater Flow in Hydrothermal Systems: A Review, Journal of Volcanology and Geothermal Research, Vol. 437, 2023, pp. 107788, https://doi.org/10.1016/j.jvolgeores.2023.107788.

[2] D. Jougnot, N. Linde, E. B. Haarder, M. C. Looms, Monitoring of Saline Tracer Movement with Vertically Distributed Self-Potential Measurements at the HOBE Agricultural Test Site, Voulund, Denmark, Journal of Hydrology, Vol. 521, 2015, pp. 314–327, https://doi.org/10.1016/j.jhydrol.2014.11.041.

[3] E. B. Voytek, H. R. Barnard, D. Jougnot, K. Singha, Transpiration- and Precipitation-Induced Subsurface Water Flow Observed Using the Self-Potential Method, Hydrological Processes, Vol. 33, No. 12, 2019, pp. 1784-1801, https://doi.org/10.1002/hyp.13453.

[4] K. Hu, D. Jougnot, Q. Huang, M. C. Looms, N. Linde, Advancing Quantitative Understanding of Self-Potential Signatures in the Critical Zone through Long-Term Monitoring, Journal of Hydrology, Vol. 585, 2020, pp. 124771, https://doi.org/10.1016/j.jhydrol.2020.124771.

[5] A. Revil, A. Jardani, The Self-Potential Method: Theory and Applications in Environmental Geosciences, Cambridge University Press, Cambridge, 2013.

[6] Y. Ozaki, H. Mikada, T. Goto, J. Takekawa, Self-Potential Inversion for the Estimation of Permeability Structure, Journal of Environmental and Engineering Geophysics, Vol. 19, No. 4, 2014, pp. 193-199, https://doi.org/10.2113/jeeg19.3.193.

[7] M. T. Graham, D. MacAllister, J. Vinogradov, M. D. Jackson, A. P. Butler, Self-Potential as a Predictor of Seawater Intrusion in Coastal Groundwater Boreholes, Water Resources Research, Vol. 54, No. 9, 2018, pp. 6055-6071, https://doi.org/10.1029/2018WR022972.

[8] M. Hidayat, M. Sarmadivaleh, J. Derksen, D. Vega-Maza, S. Iglauer, J. Vinogradov, Zeta Potential of $CO_2$-Rich Aqueous Solutions in Contact with Intact Sandstone Samples at Temperatures of 23°C and 40°C and Pressures up to 10.0 MPa, Journal of Colloid and Interface Science, Vol. 607, 2022, pp. 1226-1238, https://doi.org/10.1016/j.jcis.2021.09.076.

[9] J. Vinogradov, M. Z. Jaafar, M. D. Jackson, Measurement of Streaming Potential Coupling Coefficient in Sandstones Saturated with Natural and Artificial Brines at High Salinity, Journal of Geophysical Research: Solid Earth, Vol. 115, 2010, pp. B12204, https://doi.org/10.1029/2010JB007593.

[10] L. D. Thanh, Streaming Potential in Unconsolidated Samples Saturated with Monovalent Electrolytes, VNU Journal of Science: Mathematics and Physics, Vol. 34, No. 1, 2018, pp. 14-24, https://doi.org/10.25073/2588-1124/vnumap.4213.

[11] D. Chen, N. Arancibia-Miranda, M. Escudey, J. Fu, Q. Lu, C. H. Amon, D. Galatro, A. M. Guzmán, Nonlinear Dependence (on Ionic Strength and pH) of Surface Charge Density and Zeta Potential in Microchannel Electrokinetic Flow, Heliyon, Vol. 9, No. 10, 2023, pp. e20888, https://doi.org/10.1016/j.heliyon.2023.e20888.

[12] C. Yin, W. Guan, H. Hu, Streaming Potential Experiment on Sandstone Core Samples Based on Current Source Model under Different Sodium Chloride Solutions, Sensors, Vol. 24, No. 11, 2024, pp. 3514, https://doi.org/10.3390/s24113514.

[13] F. M. Coelho, J. Vinogradov, J. J. Derksen, L. F. M. Franco, Electrokinetic Properties of NaCl Solution via Molecular Dynamics Simulations with Scaled-Charge Electrolytes, The Journal of Chemical Physics, Vol. 161, No. 4, 2024, pp. 044508, https://doi.org/10.1063/5.0219098.

[14] P. Leroy, A. Maineult, S. Li, J. Vinogradov, The Zeta Potential of Quartz: Surface Complexation Modelling to Elucidate High Salinity Measurements, Colloids and Surfaces A: Physicochemical and Engineering Aspects, Vol. 650, 2022, pp. 129507, https://doi.org/10.1016/j.colsurfa.2022.129507.

[15] L. D. Thanh, R. Sprik, Zeta Potential in Porous Rocks in Contact with Monovalent and Divalent Electrolyte Aqueous Solutions, Geophysics, Vol. 81, No. 5, 2016, pp. D303–D314, https://doi.org/10.1190/geo2015-0571.1.

[16] F. Feldmann, E. W. Al-Shalabi, A. Hiorth, Surface Charge Change in Carbonates during Low-Salinity Imbibition, Scientific Reports, Vol. 14, 2024, pp. 13018, https://doi.org/10.1038/s41598-024-63317-z.

[17] L. D. Thanh, N. M. Hung, D. T. M. Hue, T. T. C. Thuy, Streaming Potential Coefficient Measurements in Porous Rocks Saturated by Divalent Electrolytes, VNU Journal of Science: Mathematics and Physics, Vol. 36, No. 4, 2020, pp. 76-83, https://doi.org/10.25073/2588-1124/vnumap.4501.

[18] F. D. Morgan, E. R. Williams, T. R. Madden, Streaming Potential Properties of Westerly Granite with Applications, Journal of Geophysical Research: Solid Earth, Vol. 94, No. B9, 1989, pp. 12449-12461, https://doi.org/10.1029/JB094iB09p12449.